Solid State Science and Technology, Vol. 33, No. 1 (2025) 25-33
https://doi.org/10.66514/ssst33-1-25-33

Role of High Sintering Temperature on $Pr_{0.7}Ca_{0.3}MnO_3$ Prepared via Solid-State Reaction Method

Kean Pah Lim, Xiao Tong Hon, Lik Nguong Lau, TongXin Ji, Mohd Mustafa Awang Kechik, Soo Kien Chen, Muhammad Kashfi Shabdin, Nurhidayah Mohd Hapipi, Abdul Halim Shaari*

Superconductor and Thin Film Laboratory, Department of Physics, Faculty of Science Universiti Putra Malaysia, 43400 UPM Serdang, Selangor, Malaysia

**Corresponding author: limkp@upm.edu.my*

(Received: 3 May 2025 / Revised: 4 June 2025 / Accepted: 8 June 2025 / Published online: 20 June 2025)

ABSTRACT

This study explores the effects of elevated sintering temperatures on $Pr_{0.7}Ca_{0.3}MnO_3$ samples prepared via the solid-state reaction method. XRD analysis shows that grain size increases with higher sintering temperature, while SEM images demonstrate significant microstructural alterations. At 1300 °C and 1400 °C, notable grain expansion, microcracks and melting indicate nucleation or recrystallisation stages, corresponding to consistent peak resistivity values of 11 Ω. Higher sintering temperatures generally enhance TCR due to improved grain connectivity. However, at 1400 °C, increased oxygen vacancies disturb electron hopping, resulting in a lower TCR. Thus, 1300 °C is identified as the optimal sintering temperature, yielding the highest TCR of 26.53 % K^{-1} suitable for bolometric applications.

Keywords: PCMO; microstructural change; temperature coefficient of resistance; grain boundary effect

INTRODUCTION

Perovskite manganites have emerged as a key area of study due to their high correlation between charge, spin, lattice and orbital degrees of freedom [1]. This unique interplay makes them highly promising for magnetic sensing or spintronic applications. Among these materials, praseodymium-based manganites, particularly $Pr_{1-x}Ca_xMnO_3$ stand out because of their narrower bandwidth and multiple magnetic phases [2]. In this work, the incorporation of calcium ions is expected to introduce some empty e_g orbitals by converting some Mn^{3+} to Mn^{4+} [3]. This structural change, including alterations in both Mn-O-Mn bond lengths and Mn-O bond angles, significantly affects the electronic transition between Mn^{3+} and Mn^{4+}, thereby changing their magnetic behaviour. As a representative low-bandwidth manganite, $Pr_{1-x}Ca_xMnO_3$ experiences a reduced

ferromagnetic range and loss of metallicity [4]. It undergoes a transition from ferromagnetic metallic phase to a charged-ordered antiferromagnetic insulating phase under certain condition [5]. By controlling the doping level at $x = 0.3$, $Pr_{0.7}Ca_{0.3}MnO_3$ (PCMO) marks the threshold between a ferromagnetic insulating ground state and a charge-ordered antiferromagnetic ground state, accompanied by colossal magnetoresistance linked to a metamagnetic transition [6].

The solid-state reaction method is a cornerstone in manganite preparations, celebrated for its efficiency in producing desired structures [7]. This approach is not only cost-effective and straightforward, but also offer several advantages in material synthesis, including simplicity in composition control [8]. Despite these benefits, there remains a research gap regarding the effect of exceptionally high sintering temperatures, particularly up to 1400 °C, on the physical behaviour of manganite samples. Previous research has largely constrained their investigation to sintering temperature up to 1100 °C – 1200 °C [9-11] . Hence, this study undertakes a comprehensive exploration of PCMO manganites sintered at elevated temperatures ranging from 1000 °C to 1400 °C to elucidate the microstructural changes that subsequently influence their electrical behaviour.

Numerous studies demonstrate that the modification of microstructures and physical properties of perovskite manganites is strongly dependent on the preparation conditions, including sintering temperature and duration. For instance, Zhu et al. found that higher sintering temperatures help improve the crystallinity of $La_{0.7}Ca_{0.25}K_{0.05}MnO_3$ films and reduce the MnO_6, octahedral distortions, resulting in higher resistivity and shifting the T_{MI} towards lower temperature [12]. Besides, Wang et al. also discovered that raising the sintering temperatures facilitates grain growth, improves electron hopping, enhances double-exchange interactions, and boosts the temperature coefficient of resistance (TCR) in their preparation of $La_{0.67}Ca_{0.33}MnO_3$ polycrystalline ceramics through sol-gel technique [13]. Therefore, it is anticipated that optimising the sintering temperature during sample preparation can lead to higher TCR in this work. Hence, the objective of this work is to explore the influence of sintering temperatures on the structural, microstructural and electrical behaviours of $Pr_{0.7}Ca_{0.3}MnO_3$ in order to determine the optimal condition for achieving maximum TCR performance.

MATERIALS AND METHODS

In this work, $Pr_{0.7}Ca_{0.3}MnO_3$ was synthesised using solid-state reaction method. The precursor powder used were Pr_6O_{11} (Strem Chemicals, 99.9%), $CaCO_3$ (Alfa Aesar, 99.95%) and $MnCO_3$ (Sigma-Aldrich, ≥ 99.9%). Stoichiometric amounts of these starting powders were mixed with analytical-grade acetone using the ball-milling technique for 24 h. The mixture was then dried in an oven at 70 °C for another 24 h. Next, the dried powder was calcined at 900 °C for 12 h before undergoing grinding and sieving processes. The resulting powder was pressed into pellets and sintered at temperatures ranging from 1000 °C to 1400 °C for 24 h. Hereafter, the samples will be designated as PCMO10, PCMO11, PCMO12, PCMO13, PCMO14, corresponding to their respective sintering temperatures in this manuscript. For sample characterisation, the phase formation was identified by an X-ray diffractometer (XRD, X'Pert PRO PW 3040), while the microstructural properties were observed using scanning electron microscopy (SEM, Phenom ProX Desktop SEM). Furthermore, electrical behaviour was examined using a

standard four-point probe method via Hall effect measurement system (HMS, Lakeshore 7604).

RESULTS AND DISCUSSION

Structural analysis

Figure 1 displays the XRD patterns of $Pr_{0.7}Ca_{0.3}MnO_3$ (PCMO) samples sintered at various temperatures. Upon indexing, all samples exhibited a pure PCMO phase with an orthorhombic structure and Pnma space group (ICSD reference code: 98-006-0514). As shown in Table 1, the Mn-O bond angles and Mn-O-Mn bond lengths showed negligible variations despite the different sintering temperatures. Additionally, crystallite sizes were calculated using Scherrer's equation given by [14]:

$$D = (k\,\lambda)/(\beta \cos \theta)$$

where k represents the crystallite shape factor (0.9), λ is the X-ray wavelength (1.5406 Å), β denotes the peak width at half maximum intensity (FWHM) and θ stands for the Bragg angle. It was observed that there is a general increase in crystallite size with higher sintering temperature due to the enhanced diffusion effects [15]. However, PCMO13 demonstrated a slightly larger crystallite size compared to PCMO14. This difference may be attributed to the higher goodness of fit values influenced by additional factors affecting the measurements [16].

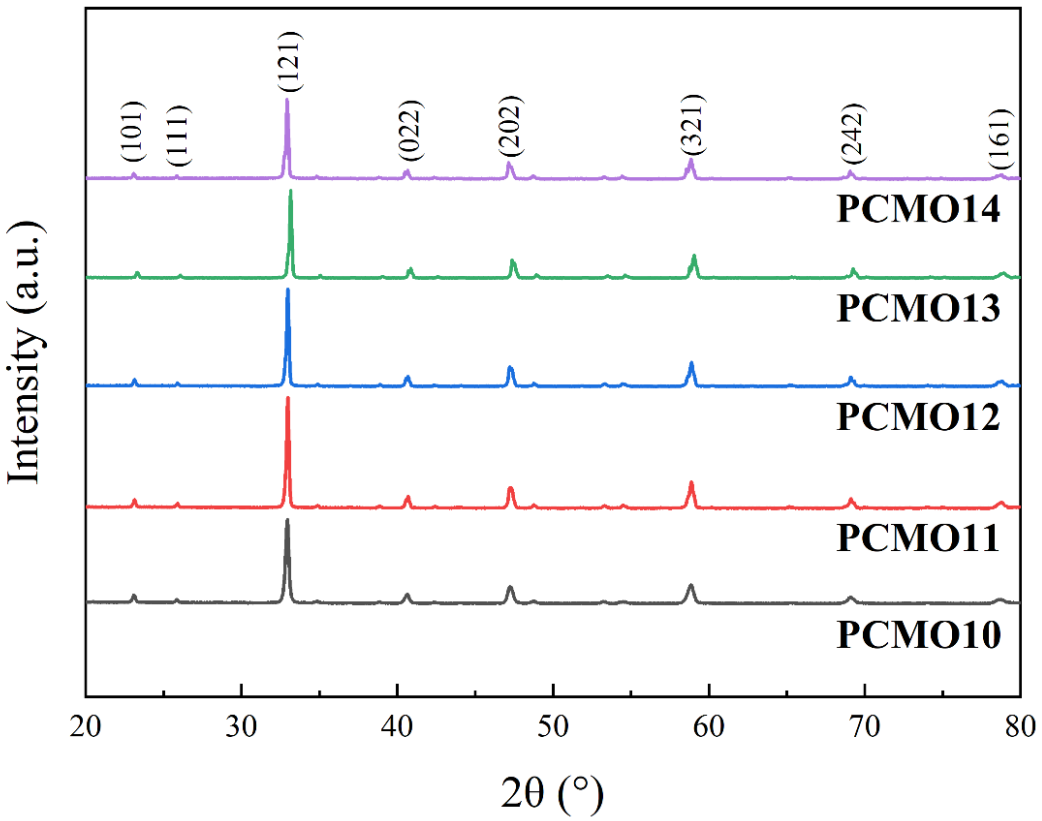

Figure 1. XRD patterns of PCMO samples sintered at different temperatures

Table 1. Rietveld refinement data of PCMO samples sintered at different temperatures

Sample code	PCMO10	PCMO11	PCMO12	PCMO13	PCMO14
Sample	Praseodymium calcium manganese oxide (PCMO)				
Reference code	98-006-0514				
Structure type	Orthorhombic				
Space group	Pnma (62)				
a (Å)	5.460	5.457	5.459	5.464	5.463
b (Å)	7.671	7.671	7.671	7.676	7.671
c (Å)	5.431	5.429	5.429	5.433	5.430
V (Å^3)	227.451	227.287	227.358	227.874	227.568
Mn_1-O_1 (Å)	1.957	1.956	1.956	1.958	1.957
Mn_1-O_1 (Å)	1.977	1.976	1.977	1.978	1.978
Mn_1-O_2 (Å)	1.959	1.959	1.959	1.960	1.959
∠Mn_1-O_1-Mn_1 (°)	156.385	156.381	156.382	156.384	156.388
∠Mn_1-O_2-Mn_1 (°)	156.515	156.522	156.521	156.521	156.516
R_{EXP} (%)	3.391	3.350	3.516	3.708	3.683
R_P (%)	3.064	3.630	3.867	4.173	3.859
R_{WP} (%)	3.899	4.710	5.061	5.546	5.352
Goodness of fit, χ^2	1.322	1.977	2.073	2.237	2.112
FWHM values (°)	0.223	0.166	0.156	0.096	0.098
Crystallite size (nm)	47.9	71.4	78.2	180.2	172.6

Microstructural analysis

Figure 2 illustrates the surface morphologies of the PCMO samples, revealing an increase in grain size increases with rising sintering temperature. In PCMO10, grain agglomeration with indistinct boundaries is observed, likely due to insufficient thermal energy for complete compound formation [17]. As the sintering temperature increases, grain growth is initiated, leading to reduced porosity and improved density [18]. Furthermore, higher sintering temperatures tend to increase the oxygen demand, resulting in oxygen deficiency and contributing to grain enlargement [19]. At sintering temperature of 1100 °C and 1200 °C, neck formation and clear grain boundaries appear in PCMO11, while PCMO12 shows a more compact structure with fewer pores due to densification [20]. A significant finding from this work is that thermal expansion of the samples becomes apparent when the sintering temperature reaches 1300 °C, possibly caused by extensive grain growth and nearly complete densification at these extremely higher temperatures [21]. This effect is more pronounced in sample PCMO14, which exhibits significantly larger grain sizes as grain growth accelerates with increasing sintering temperature. Additionally, the micrographs suggest that both PCMO13 and PCMO14 are likely experiencing nucleation

or recrystallisation, as indicated by presence of microcracks and signs of melting [22]. This stage also marks the appearance of closed pores and densification as the sintering temperature approaches the secondary recrystallisation temperature.

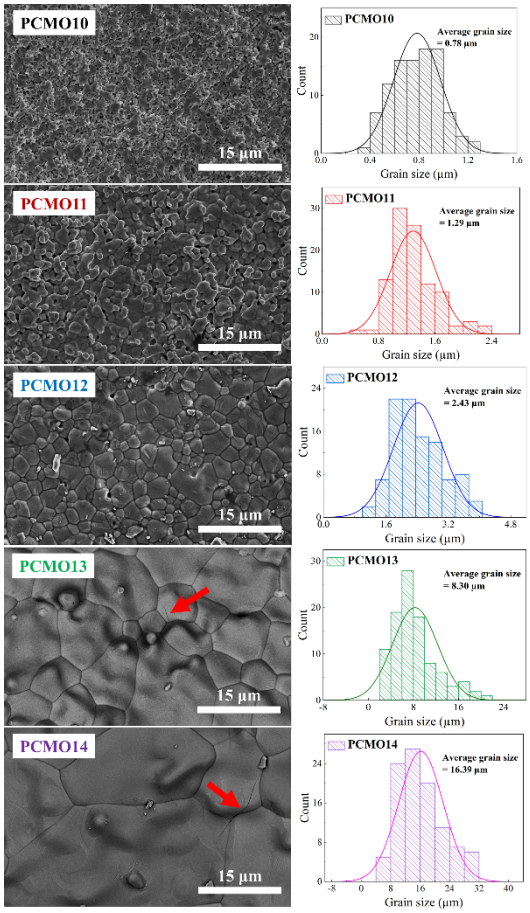

Figure 2. SEM micrographs and the grain size distribution histograms of PCMO samples sintered at different temperatures

Resistivity measurement

Figure 3 depicts the temperature-dependent resistivity measurements of the PCMO samples sintered at different temperatures. The peak resistivity values decrease significantly from 37 Ω to 13 Ω and then to 11 Ω, as the sintering temperature increases from 1000 °C to 1100 °C and subsequently to 1200 °C. This reduction can be attributed to the enhanced connectivity between the grains and decreased porosity resulting from grain growth [23]. Additionally, the magnetic inhomogeneities at the grain boundaries act as strong scattering centres due to the higher magnetic disorders compared to the cores [24]. As grain growth progresses, the influence of grain boundaries diminishes, leading to a drastic decrease in resistivity. Notably, when samples are further sintered at 1300 °C and 1400 °C, the resistivity values remain almost unchanged (≈ 11 Ω). This stability may occur because the samples achieve maximum densification and minimized porosity at specific sintering temperatures. Beyond this point, any further increment in temperature does not significantly improve the density or alter defects concentration (such as oxygen vacancies), resulting in unchanged resistivity in PCMO13 and PCMO14.

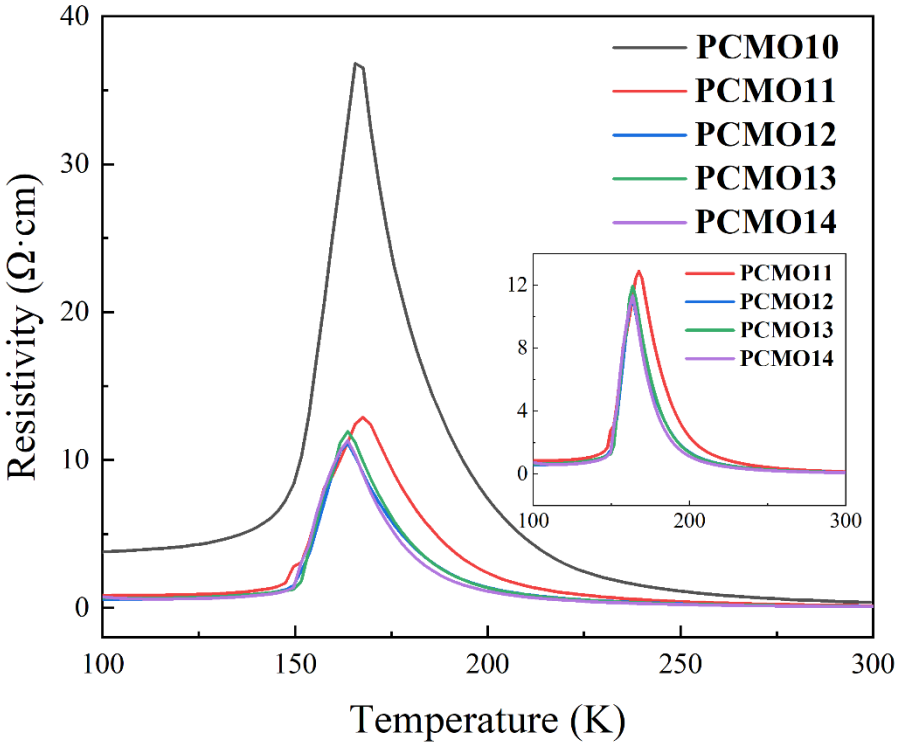

Figure 3. ρ-T curve of PCMO samples sintered at different temperatures

Temperature coefficient of resistance

The temperature coefficient of resistance (TCR) in manganites is another essential parameter that reflects the sensitivity of magnetic sensors, especially infrared bolometers [25]. It demonstrates the strong relationship between changes in resistivity of manganites with temperature fluctuations and can be defined using following equation [26]:

$$TCR\ (\%) = [\ (1/\rho)\ \times\ (d\rho/dT)\ ] \times 100\%$$

As shown in Figure 4 the TCR values initially increase with rising sintering temperatures before eventually declining. Compared to other samples, PCMO10 exhibits a notably smaller TCR value, measured at 11.51% K^{-1}. This difference can be related to the stronger grain boundary effect and weaker double exchange interactions, resulting from smaller grain sized formed at lower sintering temperatures [13]. As the sintering temperature increases, TCR values gradually improve due to better grain connectivity and reduced influence of grain boundary effects [27]. However, in PCMO14, the oxygen vacancies disturb spin polarisation and limit electron hopping processes, thereby weakening the double exchange mechanism and leading to a lower TCR value of 24.33 % K^{-1} [28]. Hence, it can be deduced that 1400 °C exceeds the melting point of PCMO in this study, while 1300 °C is identified as the optimal sintering temperature for infrared sensor in bolometric applications, recording the highest TCR value at 26.53 % K^{-1}.

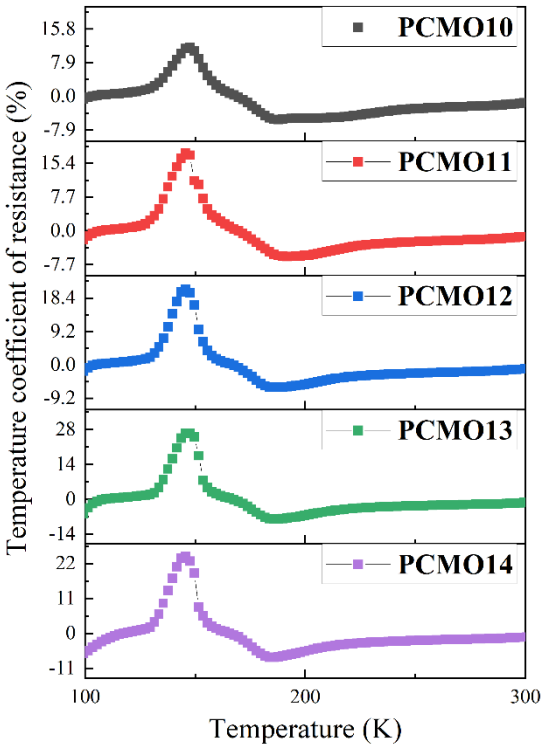

Figure 4. TCR plots of PCMO samples sintered at different temperatures

CONCLUSION

As sintering temperature increases, both crystallite and grain sizes increase as a result of the diffusion effect. SEM micrographs reveal that higher sintering temperatures induce significant microstructural changes, including the formation of larger grains, increased density and reduced porosity. Notably, at 1300 °C and 1400 °C, significant grain expansion, along with signs of melting and microcracks, suggests proximity to nucleation or recrystallisation points. This observation is consistent the resistivity measurement, which shows consistent peak resistivity values of 11 Ω at these temperatures. Typically, increasing sintering temperatures lead to lower resistivity by improving the grain connectivity, which also improves the temperature coefficient of resistance (TCR). However, at 1400 °C, exceeding the melting point of PCMO introduces additional defects and disrupts the electron hopping process, resulting in a lower TCR of 24.33 % K^{-1}. Thus, the highest TCR of 26.53 % K^{-1} was achieved at sintering temperature of 1300 °C in this work.

ACKNOWLEDGEMENTS

This research was fully funded and supported by the Universiti Putra Malaysia research grants (GP/2023/9753000). The authors are grateful to the support staff who assisted in the characterisation measurements and for the facilities provided by Universiti Putra Malaysia.

REFERENCES

1. Bennett MC, Hu G, Wang G, Heinonen O, Kent PRC, Krogel JT, Ganesh P. Origin of metal-insulator transitions in correlated perovskite metals. *Phys Rev Res*. 2022;4(2):L022005.
2. Majumdar S, Huhtinen H, Granroth S, Paturi P. Evolution of structural and magnetic properties with varying oxygen content in low-bandwidth manganite $Pr_{0.9}Ca_{0.1}MnO_3$ thin films. *J Phys Condens Matter*. 2012;24(20):206002.
3. L. Zhou, G. Song, Y. Zhang, Q. Liu, S. Li, J. Yang, W. Bai, X. Tang. The effect of stress on the magnetic properties of sol–gel-derived $Pr_{0.9}Ca_{0.1}MnO_3$ thin films. *J Mater Sci Mater Electron*. 2021;32(18):23126–33.
4. Tomioka Y, Asamitsu A, Kuwahara H, Moritomo Y, Tokura Y. Magnetic-field-induced metal-insulator phenomena in $Pr_{1-x}Ca_xMnO_3$ with controlled charge-ordering instability. *Phys Rev B*. 1996;53(4):R1689.
5. Fiebig M, Miyano K, Tomioka Y, Tokura Y. Visualization of the local insulator-metal transition in $Pr_{0.7}Ca_{0.3}MnO_3$. *Science*. 1998;280(5371):1925–8.
6. Tikkanen J, Huhtinen H, Paturi P. Oxygen-sintered (Pr, Ca)MnO_3: Structure and magnetism at high Ca concentrations. *J Alloys Compd*. 2015;635:41–7.
7. Ezaami A, Nasser NO, Cheikhrouhou-Koubaa W, Koubaa M, Cheikhrouhou A, Hlil E. Physical properties of $La_{0.7}Ca_{0.2}Sr_{0.1}MnO_3$ manganite: a comparison between sol–gel and solid state process. *J Mater Sci Mater Electron*. 2017;28:3648–58.
8. Ko D, Mhin S. Effect of one step solid state reaction route on the semiconductor behavior of the spinel (Ni, Co, and Mn)O_4 to be used as temperature sensor. *Sensors*. 2023;23(12):5380.
9. Nadig PR, Murari M, Daivajna MD. Influence of heat sintering on the physical properties of bulk $La_{0.67}Ca_{0.33}MnO_3$ perovskite manganite: role of oxygen in tuning the magnetocaloric response. *Phys Chem Chem Phys*. 2024;26(6):5237–52.
10. L.N. Lau, K.P. Lim, A.N. Ishak, M.M. Awang Kechik, S.K. Chen, N.B.y. Ibrahim, M. Miryala, M. Murakami, A.H. Shaari. The physical properties of submicron and nano-grained $La_{0.7}Sr_{0.3}MnO_3$ and $Nd_{0.7}Sr_{0.3}MnO_3$ synthesised by sol–gel and solid-state reaction methods. *Coatings*. 2021;11(3):361.
11. Ayaş AO, Kandemir A, Çetin SK, Akça G, Akyol M, Ekicibil A. Investigation of the effect of sintering temperature on structural, magnetic and magnetocaloric properties in $PrCaMn_2O_6$ double perovskite manganite system. *J Mater Sci Mater Electron*. 2022;33(10):7357–70.
12. X. Zhu, X. Gu, J. Han, J. Jiang, Z. Pan, J. Wang, Z. Chen, X. Liu. Tuning strain-stress and electron-lattice effects to enhance electrical transport properties of $La_{0.7}Ca_{0.25}K_{0.05}MnO_3$ films via optimizing sintering temperatures. *Ceram Int*. 2024;50(4):6969–78.
13. Z. Wang, J. Jiang, X. Gu, J. Han, X. Liang, Y. Wang, Z. Chen, H. Wang, X. Liu. Large temperature coefficient of resistivity (TCR) of $La_{0.67}Ca_{0.33}MnO_3$ polycrystalline ceramics improved by optimizing sintering temperatures. *Ceram Int*. 2024;50(7):10160–70.
14. Scherrer P. Bestimmung der Grösse und inneren Struktur von Kolloidteilchen mittels Röntgenstrahlen. *Nachr Ges Wiss Göttingen*. 1918;2:8–100.
15. B. Munisha, B. Mishra, J. Nanda, N.K. Sahoo, D. Ghosh, K. Sankaran, S. Suman. Enhanced photocatalytic degradation of 4-nitrophenol using polyacrylamide assisted

Ce-doped $YMnO_3$ nanoparticles. *J Rare Earths*. 2023;41(10):1541–50.
16. Canchanya-Huaman Y, Mayta-Armas AF, Pomalaya-Velasco J, Bendezú-Roca Y, Guerra JA, Ramos-Guivar JA. Strain and grain size determination of CeO_2 and TiO_2 nanoparticles: comparing integral breadth methods versus Rietveld, μ-Raman, and TEM. *Nanomaterials*. 2021;11(9):2311.
17. Malti A, Kardani A, Montazeri A. An insight into the temperature-dependent sintering mechanisms of metal nanoparticles through MD-based microstructural analysis. *Powder Technol*. 2021;386:30–9.
18. Cheng Q, Wang Y, Zhang J, Conejo AN, Liu Z. The grain growth and grain boundary migrations during solid-phase sintering of Fe_2O_3: experiments and simulations. *Chem Eng Sci*. 2022;262:118038.
19. Mleiki A, Khlifi A, Rahmouni H, Guermazi N, Khirouni K, Hlil E, Cheikhrouhou A. Magnetic and dielectric properties of Ba-lacunar $La_{0.5}Eu_{0.2}Ba_{0.3}MnO_3$ manganites synthesized using sol-gel method under different sintering temperatures. *J Magn Magn Mater*. 2020;502:166571.
20. M.R. Mazlan, N.H. Jamadon, A. Rajabi, A.B. Sulong, I.F. Mohamed, F. Yusof, N.A. Jamal. Necking mechanism under various sintering process parameters – a review. *J Mater Res Technol*. 2023;23:2189–201.
21. Babalola BJ, Ayodele OO, Olubambi PA. Sintering of nanocrystalline materials: sintering parameters. *Heliyon*. 2023;9(3):e14070.
22. Besisa DH, Ewais EM. Black zirconia composites with enhanced thermal, optical and mechanical performance for solar energy applications. *Sol Energy Mater Sol Cells*. 2021;225:111063.
23. W. Hizi, H. Rahmouni, N.E. Gorji, A. Guesmi, N. Ben Hamadi, L. Khezami, E. Dhahri, K. Khirouni, M. Gassoumi. Impact of sintering temperature on the electrical properties of $La_{0.9}Sr_{0.1}MnO_3$ manganite. *Catalysts*. 2022;12(3):340.
24. Das S, Chowdhury P, Rao TG, Das D, Bahadur D. Influence of grain size and grain boundaries on the properties of $La_{0.7}Sr_{0.3}Co_xMn_{1-x}O_3$. *Solid State Commun*. 2002;121(12):691–5.
25. Yu X, Jin S, Guan X, Yan Y, Wu K, Zhao L, Liu X. Large temperature coefficient of resistivity (TCR) of $La_{1-x}Ca_xMnO_3$ films prepared by spin-coating method. *J Alloys Compd*. 2022;890:161788.
26. M. Rajeswari, R. Shreekala, A. Goyal, S. Lofland, S. Bhagat, K. Ghosh, R. Sharma, R. Greene, R. Ramesh, T. Venkatesan. Correlation between magnetic homogeneity, oxygen content, and electrical and magnetic properties of perovskite manganite thin films. *Appl Phys Lett*. 1998;73(18):2672–4.
27. Wu D, Zhang H, Li L, Qi L, Gao Y, Yang Y, Chen Q. Effect of sintering temperature on structure and electrical transport properties of $La_{0.7}Ca_{0.26}Na_{0.04}MnO_3$ ceramics. *Ceram Int*. 2021;47(9):12716–24.
28. L. Qi, Y. Li, P. Yu, X. Wang, Y. Li, Y. Gao, Y. Yang, D. Wu, H. Zhang, Q. Chen. Exploring the electrical transport properties of $La_{0.67}Ca_{0.33}MnO_3$ at different sintering temperatures. *J Mater Sci Mater Electron*. 2021;32(11):14164–73.